nature neuroscience

Intracortical multiplication of thalamocortical signals in mouse auditory cortex

Ling-yun Li[1,2], Ya-tang Li[1,2], Mu Zhou[1,2], Huizhong W Tao[1,3] & Li I Zhang[1,4]

Cortical processing of sensory information begins with the transformation of thalamically relayed signals. We optogenetically silenced intracortical circuits to isolate thalamic inputs to layer 4 neurons and found that intracortical excitation linearly amplified thalamocortical responses underlying frequency and direction selectivity, with spectral range and tuning preserved, and prolonged the response duration. This signal pre-amplification and prolongation enhanced the salience of thalamocortically relayed information and ensured its robust, faithful and more persistent representation.

Across sensory modalities, information undergoes lamina-specific processing in the cortex[1,2]. Layer 4 is the major thalamo-recipient layer[1–4]. Instead of passively receiving the afferent input, it has been proposed to have an active role in thalamocortical transformation by integrating local and distant intracortical excitatory inputs[5–7]. Attempts to dissect the thalamocortical and intracortical excitatory inputs to individual cortical neurons have been made, but there are technical limitations involved in silencing the cortex in a specific and reversible manner, and the precise functional role of intracortical excitation remains poorly understood[5–10]. Specifically, in the auditory cortex, the manner in which the thalamocortical and intracortical excitation determine the spectral integration of cortical neurons and the nature of their quantitative relationship remain controversial[4,11–13]. Using an optogenetic approach[14–16] in the mouse primary auditory cortex (A1), we silenced cortical circuits in a reversible manner by activating parvalbumin (PV)-expressing inhibitory neurons. We were therefore able to isolate the thalamocortical and intracortical excitation onto the same neuron and quantitatively examine their relationship.

We took advantage of Cre-*loxP* recombination to express channelrhodopsin-2 (ChR2) in PV$^+$ neurons. An adeno-associated viral vector AAV2/9-EF1α-DIO-hChR2-EYFP was injected into the A1 of *Pvalb-cre* tdTomato transgenic mice (Online Methods). ChR2 was expressed specifically in PV$^+$ neurons, as shown by the colocalization of EYFP and tdTomato fluorescence in cortical slices 2 weeks after the injection (**Fig. 1a**,**b**). Using *in vivo* two-photon imaging–guided recording from tdTomato-labeled PV$^+$ neurons, we found that illuminating the exposed A1 surface with blue LED light (470 nm) markedly increased firing of these neurons (**Fig. 1c**) in each of consecutive trials (**Supplementary Fig. 1a**). In contrast, LED illumination completely blocked spiking of excitatory neurons recorded in both layers 4 and 6 (**Fig. 1d**) as a result of a large inhibitory current caused by the activation of PV$^+$ neurons (**Fig. 1d**).

Although tone-evoked spike responses were eliminated in layer 6 under LED illumination, those of thalamic neurons in the ventral medial geniculate body (MGBv) of the same mouse were apparently unaffected (**Fig. 1e**). Both multi-unit and single-cell loose-patch recordings revealed that the average evoked firing rate (**Fig. 1f**) and the frequency tuning properties (**Supplementary Fig. 2**) in the MGBv remained unchanged after cortical silencing, consistent with previous observations[12,17–19].

We next examined the relative contributions of thalamocortical and intracortical excitatory circuits to frequency tuning by applying brief tone stimuli. Whole-cell voltage-clamp recordings were made from layer 4 excitatory neurons, with their membrane potential clamped at the reversal potential of inhibitory currents (Online Methods). In the same cell, thalamocortical response was isolated from the total excitatory response by reversibly silencing the cortex. Control trials with the tone stimulus only (LED off) and trials with the tone stimulus coupled with LED illumination (LED on) were alternated. As shown by two example cells (**Fig. 2a–d**), LED illumination decreased the peak amplitudes of excitatory responses at all of the effective tone frequencies (**Fig. 2a**,**c**). Linear fitting revealed that response amplitude was reduced by a similar fraction across different frequencies, resulting in largely unchanged frequency tuning (**Fig. 2b**,**d**). The onset latencies of tone-evoked responses exhibited a frequency-dependent modulation, with the shortest latency occurring at the best frequency and the longest latencies occurring at frequencies distant from the best frequency. The latency was not apparently different in the presence of LED illumination (**Fig. 2b**,**d**), supporting the notion that, across effective frequencies, thalamocortical input generates the earliest excitatory response in cortical cells.

For 14 layer 4 excitatory neurons, we did not observe a notable change in frequency tuning of excitation after cortical silencing, as quantified by the total frequency range (**Fig. 2e**) and half-maximum bandwidth of tuning curve (**Fig. 2f**), as well as by the best frequency and tuning sharpness (**Supplementary Fig. 3a**,**b**). The linear relationship between thalamocortical and intracortical excitatory responses was strong in all of the cells, with the correlation coefficients all being higher than 0.74 (**Supplementary Table 1**). Similar observations were made when the total integrated charge of excitatory current was measured (**Supplementary Fig. 4**).

To examine changes in response magnitude, we plotted the average peak amplitude of all of the responses in the effective frequency

[1]Zilkha Neurogenetic Institute, Keck School of Medicine, University of Southern California, Los Angeles, California, USA. [2]Graduate Programs, Keck School of Medicine, University of Southern California, Los Angeles, California, USA. [3]Department of Cell and Neurobiology, Keck School of Medicine, University of Southern California, Los Angeles, California, USA. [4]Department of Physiology and Biophysics, Keck School of Medicine, University of Southern California, Los Angeles, California, USA. Correspondence should be addressed to L.I.Z. (liizhang@usc.edu).

Received 28 April; accepted 27 May; published online 11 August 2013; doi:10.1038/nn.3493

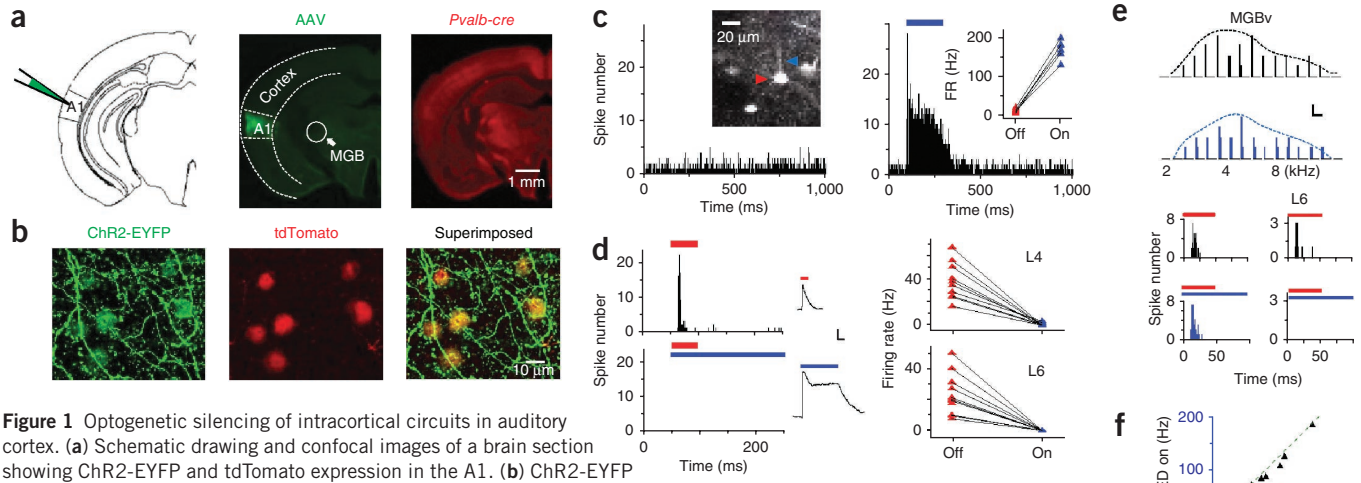

Figure 1 Optogenetic silencing of intracortical circuits in auditory cortex. (**a**) Schematic drawing and confocal images of a brain section showing ChR2-EYFP and tdTomato expression in the A1. (**b**) ChR2-EYFP was expressed in tdTomato-labeled PV$^+$ neurons. (**c**) Peri-stimulus spike time histogram (PSTH) for an example PV$^+$ cell without (left) and with (right) LED illumination (blue bar, 200 ms). Left inset, two-photon image of the cell-attached recording from the PV$^+$ cell. Right inset, average firing rates in LED off (red) and LED on (blue) trials for five PV$^+$ cells. FR, firing rate. (**d**) Left, PSTH of a layer 4 excitatory neuron to tone stimuli (red bar) and to combined tone and LED stimulation (blue bar). Middle, tone-evoked inhibitory current of an example cell (top) and LED-evoked inhibitory current in the same cell (bottom). Scale bars represent 80 pA and 100 ms. Right, summary of tone-evoked firing rates without (red) and with (blue) LED illumination in layer 4 (L4) and layer 6 (L6) cells. Line connects data for the same cell. (**e**) Top, reconstructed frequency tuning of multi-unit spikes (shown by PSTH) for a MGBv site. Black, tone stimulation only. Blue, tone combined with LED illumination. Scale bars represent 1 (count) and 100 ms. Bottom left, PSTHs of spike responses to tones (red bar) without (top) and with LED illumination (bottom). Bottom right, PSTHs for a layer 6 excitatory neuron recorded in the same mouse. (**f**) Summary of tone-evoked firing rates in single-cell loose-patch (SU) and multi-unit (MU) recordings without and with LED illumination ($P = 0.08$, paired t test, $n = 19$).

range in LED on trials and that in control (LED off) trials (**Fig. 2g**). A scaling factor was calculated as the average peak amplitude in LED on trials divided by that in control trials. The average scaling factor was 0.41 ± 0.15 (mean ± s.d.), indicating that, on average, thalamocortical input was amplified by about 2.4-fold. The amplification factor for responses around the best frequency was not notably different from that at frequencies distant from the best frequency (**Supplementary Fig. 3c**), further indicating that thalamocortical responses were amplified linearly by intracortical excitatory inputs. In addition, the response duration was substantially reduced after cortical silencing (**Fig. 2h**). The scaling factor based on integrated charge (average 0.25 ± 0.08, corresponding to a fourfold amplification) was smaller than that based on peak amplitude, likely as a result of the recruitment of late-arriving intracortical excitation. Thus, intracortical circuits have both amplified and prolonged tone-evoked excitatory currents.

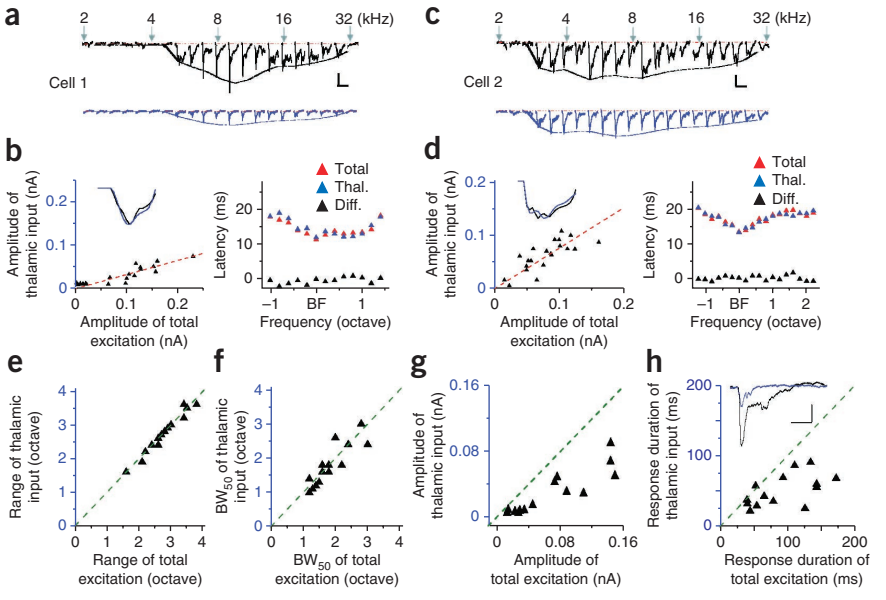

Figure 2 Intracortical input linearly amplifies frequency-tuned thalamocortical input. (**a**) Average tone-evoked excitatory currents in an example cell at different frequencies without (black) and with (blue) LED illumination. The envelope curve outlines the frequency tuning of peak amplitude. Scale bars represent 0.05 nA and 200 ms. (**b**) Left, peak amplitude of thalamic input versus total excitation evoked by the same tone stimulus. Linear fitting: $r = 0.91$, slope = 0.32, $P < 10^{-8}$, one-tail. Inset, the two envelope curves from **a** (normalized and superimposed). Right, onset latencies of thalamocortical (blue) and total (red) excitatory responses at different frequencies. BF, best frequency. (**c**,**d**) Another example cell. Scale bars represent 0.035 nA and 200 ms. Linear fitting: $r = 0.77$, slope = 0.76, $P = 3.4 \times 10^{-6}$, one-tail. (**e**) Total frequency range of thalamic input versus total excitation (2.74 ± 0.61 versus 2.79 ± 0.61 octave, $P = 0.38$, Wilcoxon signed-rank test). Each data point represents one cell. (**f**) Half-maximum bandwidth (BW_{50}) of thalamic input versus total excitation (1.79 ± 0.61 versus 1.84 ± 0.57, $P = 0.49$, paired t test). (**g**) Average peak amplitude of thalamic input versus total excitation (0.03 ± 0.03 versus 0.07 ± 0.05 nA, $P = 1.9 \times 10^{-4}$, paired t test). (**h**) Response duration of thalamic input (measured at 10% of the maximal amplitude of best frequency tone responses) versus total excitation (51.17 ± 22.06 versus 92.99 ± 44.8 ms, $P = 3.66 \times 10^{-4}$, Wilcoxon signed-rank test). Inset, average response traces without (black) and with (blue) LED illumination of an example cell. Scale bars represent 0.04 nA and 50 ms.

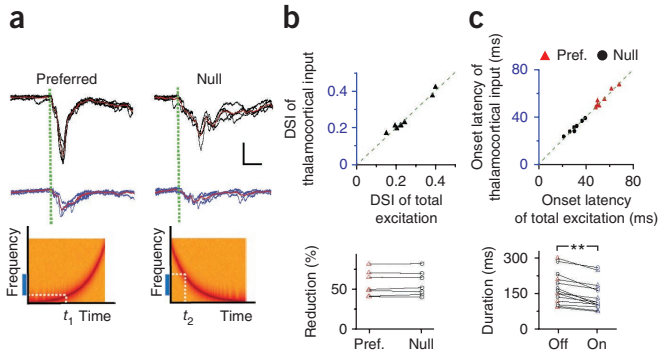

Figure 3 Intracortical input preserves direction tuning of thalamocortical input. (**a**) Top, superimposed excitatory currents and their average (red) evoked by upward and downward sweeps in an example cell without (upper) and with (lower) LED illumination. Green dotted lines mark the response onset. Scale bars represent 0.04 nA and 20 ms. Bottom, spectrograms of upward and downward frequency-modulated sweeps. Blue bars indicate the effective frequency range (frequency receptive field). t_1 and t_2 mark the times at which the frequency-modulated sweeps hit its boundary. (**b**) Top, DSI of thalamocortical input versus total excitation (0.26 ± 0.03 versus 0.26 ± 0.03, $P = 0.58$, Wilcoxon signed-rank test, $n = 7$). Bottom, percentage reduction of peak response amplitude after cortical silencing for the preferred and null directional stimuli (0.57 ± 0.05 versus 0.58 ± 0.05, $P = 0.97$, paired t test). (**c**) Top, onset latency of thalamocortical input versus total excitatory input for the preferred and null directional stimuli (preferred direction, 55.02 ± 2.56 versus 55.28 ± 2.58 ms, $P = 0.74$, paired t test; null direction, 31.38 ± 2.09 versus 31.56 ± 1.87 ms, $P = 0.75$, paired t test, $n = 7$). Bottom, response duration measured at the level of 10% of the maximal amplitude without (off) and with (on) LED illumination (170.39 ± 61.63 versus 138.36 ± 55.14 ms, $^{**}P = 1.22 \times 10^{-4}$, Wilcoxon signed-rank test, $n = 14$).

We further compared direction tuning of thalamocortical input and total excitation, by reversibly silencing the cortex, to determine how much of a direction bias that is already present in excitatory inputs to layer 4 neurons[4,20] can be attributed to thalamocortical relay. The excitatory response of an example cell exhibited a clear preference to the upward-directed frequency-modulated sweep (changing from low to high frequency; **Fig. 3a**). In the presence of LED illumination, response amplitudes to both the upward and downward sweeps were reduced, and the preference to the upward sweep was sustained. In a total of seven cells that showed a clear direction bias in their excitatory responses, we found that direction tuning was preserved after cortical silencing, as quantified by a direction selectivity index (DSI; **Fig. 3b**). This is a result of the fact that the responses to upward and downward sweeps were reduced by a similar factor (**Fig. 3b**). Measurements of both peak response amplitude and integrated charge (**Supplementary Fig. 5**) of excitatory current revealed that thalamic neurons provided direction-biased input into the cortex and that intracortical excitation amplified this thalamocortical signal without affecting the inherited direction tuning.

Finally, we found that the onset latencies of sweep responses did not change for either direction after cortical silencing (**Fig. 3c**). The onset latency provided information on the boundary of the frequency receptive field (**Fig. 3a**). The unchanged onset latencies indicated that the receptive field boundaries on both the low- and high-frequency sides were preserved. This is consistent with the finding that the spectral range was set by thalamocortical input (**Fig. 2e**). Similar to the tone-evoked responses, the temporal durations of sweep responses at both the preferred and null directions were reduced after cortical silencing (**Fig. 3c**), indicating that the recruitment of intracortical excitatory inputs also prolonged sweep responses.

Although the functional properties of neurons in the recipient layers of sensory cortices are generally considered to be determined by the convergence of thalamocortical connections[5–7,9,11], the role of intracortical excitatory circuits in transforming the thalamocortical signals remains unclear[2–4,12]. The optogenetic approach that we used overcomes the technical barriers[4,11,12] present in previous studies. The specificity and reversibility of optical stimulation allows the thalamocortical and intracortical components of synaptic excitation to be more faithfully revealed in individual cells. Our results indicate that intracortical excitation linearly amplifies the received thalamocortical signals without recruitments of additional spectral information through horizontal intracortical connections. Furthermore, for excitatory responses to both frequency-modulated sweep and tone stimuli, intracortical circuits prolonged their time course, likely as a result of recruitment of late-arriving polysynaptic excitatory inputs. Thus, analogous to a preamplifier, intracortical excitatory circuits have an active role in increasing the gain and duration of thalamocortical input signals, leading to a great enhancement of the signal-to-noise ratio and a robust and faithful representation of thalamically conveyed information.

METHODS

Methods and any associated references are available in the online version of the paper.

Note: Any Supplementary Information and Source Data files are available in the online version of the paper.

ACKNOWLEDGMENTS

This work was supported by grants from the US National Institutes of Health (DC008983 to L.I.Z., EY019049 to H.W.T.) and the David and Lucile Packard Foundation (L.I.Z.).

AUTHOR CONTRIBUTIONS

L.I.Z. conceived and supervised the study. L.L., Y.L. and M.Z. performed the experiments. L.L., H.W.T. and L.I.Z. performed data analysis. H.W.T. and L.I.Z. wrote the paper.

COMPETING FINANCIAL INTERESTS

The authors declare no competing financial interests.

1. Callaway, E.M. *Annu. Rev. Neurosci.* **21**, 47–74 (1998).
2. Douglas, R.J. & Martin, K.A. *Annu. Rev. Neurosci.* **27**, 419–451 (2004).
3. Winer, J.A., Miller, L.M., Lee, C.C. & Schreiner, C.E. *Trends Neurosci.* **28**, 255–263 (2005).
4. Wu, G.K., Tao, H.W. & Zhang, L.I. *Neurosci. Biobehav. Rev.* **35**, 2094–2104 (2011).
5. Douglas, R.J., Koch, C., Mahowald, M., Martin, K.A. & Suarez, H.H. *Science* **269**, 981–985 (1995).
6. Somers, D.C., Nelson, S.B. & Sur, M. *J. Neurosci.* **15**, 5448–5465 (1995).
7. Miller, K.D., Pinto, D.J. & Simons, D.J. *Curr. Opin. Neurobiol.* **11**, 488–497 (2001).
8. Ferster, D., Chung, S. & Wheat, H. *Nature* **380**, 249–252 (1996).
9. Miller, L.M., Escabi, M.A., Read, H.L. & Schreiner, C.E. *Neuron* **32**, 151–160 (2001).
10. Bruno, R.M. & Sakmann, B. *Science* **312**, 1622–1627 (2006).
11. Kaur, S., Lazar, R. & Metherate, R. *J. Neurophysiol.* **91**, 2551–2567 (2004).
12. Liu, B.H., Wu, G.K., Arbuckle, R., Tao, H.W. & Zhang, L.I. *Nat. Neurosci.* **10**, 1594–1600 (2007).
13. Happel, M.F., Jeschke, M. & Ohl, F.W. *J. Neurosci.* **30**, 11114–11127 (2010).
14. Zhang, F., Aravanis, A.M., Adamantidis, A., de Lecea, L. & Deisseroth, K. *Nat. Rev. Neurosci.* **8**, 577–581 (2007).
15. Bernstein, J.G., Garrity, P.A. & Boyden, E.S. *Curr. Opin. Neurobiol.* **22**, 61–71 (2012).
16. Olsen, S.R., Bortone, D.S., Adesnik, H. & Scanziani, M. *Nature* **483**, 47–52 (2012).
17. Sun, Y.J., Kim, Y.J., Ibrahim, L.A., Tao, H.W. & Zhang, L.I. *J. Neurosci.* **33**, 5326–5339 (2013).
18. Zhou, Y. *et al. Neuron* **65**, 706–717 (2010).
19. Zhou, Y. *et al. J. Neurosci.* **32**, 9969–9980 (2012).
20. Zhang, L.I., Tan, A.Y., Schreiner, C.E. & Merzenich, M.M. *Nature* **424**, 201–205 (2003).

ONLINE METHODS

Viral injection. All experimental procedures in this study were approved by the Animal Care and Use Committee of the University of Southern California. Adult *Pvalb-cre* × Ai14 tdTomato reporter line (Jackson Laboratory) pigmented female mice were anesthetized with 2% isoflurane (vol/vol). The area of skull over the left A1 (temporal lobe, 2.2–3.64 mm caudal to Bregma) was thinned and ~0.2-mm^2 craniotomy was performed. The virus was delivered using a beveled glass micropipette (tip diameter = 40–50 μm) attached to a microsyringe pump (World Precision Instruments). Adeno-associated viruses (AAVs) to deliver ChR2 were acquired from the University of Pennsylvania Viral Vector Core: AAV2/9.EF1α.DIO.hChR2(H134R)-EYFP.WPRE.hGH (Addgene 20298). Viral solution was injected at a volume of 100 nl per injection and at a rate of 20 nl min^{-1}. Injection was performed at two locations (2.7 and 3.2 mm caudal to Bregma) and two depths (300 and 600 μm). The diffusion of the virus in the cortex was about 800 μm from the injection site. We then sutured the scalp, and administered an analgesic (0.1 mg per kg of body weight Buprenex) to help the recovery from anesthesia.

Mouse preparation and extracellular recording from A1. Mice were allowed to recover for 2–4 weeks. Experiments were carried out in a sound-attenuation booth (Acoustic Systems). Adult viral injected mice were sedated with chlorprothixene (0.05 ml of 4 mg ml^{-1}) and anesthetized with urethane (1.2 g per kg). Local anesthesia was applied by administrating bupivacaine subcutaneously. The left auditory cortex was exposed and the ear canal on the same side was plugged. We first carried out sequential multi-unit recordings at an array of cortical sites to identify the location and the frequency gradient of the A1. Tone pips (50-ms duration, 3-ms ramp) of various frequencies (2–32 kHz, at 0.1 octave interval) and intensities (10-dB interval, seven intensities from 10 dB sound pressure level) were delivered through a calibrated free-field speaker facing the contralateral ear. The testing stimuli were presented in a pseudorandom sequence. Multi-unit spikes were recorded with a parylene-coated tungsten microelectrode (2 MΩ, FHC) at 400 μm below the pia. Electrode signals were amplified (Plexon) and band-pass filtered between 300 and 6,000 Hz. Custom LabVIEW (National Instruments) software was used to extract the spike times. The number of tone-evoked spikes was counted in a window of 10–50 ms from the onset of tone stimuli. The characteristic frequency of each recording site was defined as the tone frequency that evokes reliable responses at the lowest intensity level in the reconstructed spike tonal receptive field (TRF). A1 region was identified by its tonotopic representation of characteristic frequencies in a caudal-to-rostral (low-to-high frequency) gradient, relatively sharp spike TRFs and short onset latencies. After the pre-mapping of A1, all experiments were performed in the low-to-mid frequency (with characteristic frequency ~4–16 kHz) regions. During the mapping procedure, the cortical surface was slowly perfused with a pre-warmed artificial cerebrospinal fluid (ACSF; 124 mM NaCl, 1.2 mM NaH_2PO_4, 2.5 mM KCl, 25 mM $NaHCO_3$, 20 mM glucose, 2 mM $CaCl_2$, 1 mM $MgCl_2$). The spatial expression pattern of hChR2(H134R)-EYFP in each injected mouse was examined with a fluorescence microscope before and after the experiment. Only data from mice with EYFP expressing in the correct location were included in the analysis. In more than 200 EYFP-expressing neurons examined, all the cells were found to express tdTomato, that is, they were all PV^+ neurons.

Extracellular recording in MGBv. To map the auditory thalamus, we first carried out extracellular recordings in a three-dimensional manner by systematically varying the depth and the *x*-*y* coordinates of the tungsten electrode that penetrated the primary auditory cortical surface at an approximately right angle. We discriminated the MGBv from other auditory thalamic divisions according to its tonotopic frequency representation, relatively sharp spike TRFs and short onset latencies[21]. Afterward, multi-unit or single-cell loose-patch recordings were made around the central region of the MGBv (approximately 2.4~2.6 mm below the auditory cortical surface).

***In vivo* loose-patch and whole-cell voltage-clamp recordings.** Loose-patch and whole-cell recordings were carried out as previously described[22–24]. We used agar (3.25%) to minimize cortical pulsation. Patch pipettes (Kimax) with ~4–5 MΩ impedance were used. For whole-cell voltage-clamp recordings, the internal solution contained 125 mM cesium gluconate, 5 mM TEA-Cl, 4 mM MgATP, 0.3 mM GTP, 10 mM phosphocreatine, 10 mM HEPES, 1 mM EGTA, 2 mM CsCl, 1.5 mM QX-314, 1% biocytin or 0.1 fluorescent dextrans (pH 7.2). Recordings were made with an Axopatch 200B amplifier (Molecular Devices). The pipette capacitance and whole-cell capacitance were compensated completely, and the series resistance (15–30 MΩ) was compensated by 50–60% (100-μS lag). Signals were filtered at 2 kHz and sampled at 10 kHz. The evoked excitatory currents were resolved by clamping the cell at the reversal potential of inhibitory currents. The reversal potential (~−65 to −75 mV) was determined for each recorded neuron by systematically changing the holding voltage until LED-evoked currents disappeared. LED illumination resulted in a decrease (~30% on average) of the original input resistance (150–200 MΩ), but without changes in series resistance. Under our experimental condition, the change of input resistance would result in a small (less than 10%) change in the amplitude of recorded synaptic currents[25], which would not substantially affect our results. We specifically recorded from neurons located at 375–525 μm below the pia, corresponding to layer 4. The depth of layer 4 was determined on the basis of the fluorescence pattern in a layer 4–specific Cre line (Scnn1a-Tg3-Cre, Jackson laboratory) crossed with the Ai14 reporter line. By correlating the depth of recorded cell bodies, which were labeled by fluorescent dextrans in the intrapipette solution, with the travel distance of the electrode tip, we found that, under our experimental condition, the travel distance relatively precisely indicated the depth of recorded cells after the correction of a systemic error of 20 ± 7 μm (n = 12 penetrations)[26]. The reconstructed morphologies of biocytin-labeled neurons confirmed the layer 4 location (**Supplementary Fig. 1b**). The recorded neurons exhibited sound-evoked responses after cortical silencing, indicating that they were directly innervated by thalamic axons. For loose-patch recordings, pipettes were filled with filtered ACSF. Recording was performed in a similar way as the whole-cell recording, except that a loose seal (0.1–0.5 GOhm) was made on the cell body, allowing spikes only from the patched cell to be recorded. Spike responses were recorded under the voltage-clamp mode, with the command potential adjusted so that a 0-pA baseline current was achieved. Signals were filtered and sampled at 10 kHz. With large pipette openings (impedance ≤6MΩ), we did not record any fast-spiking neurons in our loose-patch recordings, suggesting that our recording parameters imposed a strong sampling bias toward pyramidal neurons with larger cell bodies and more extensive dendritic fields. This was further supported by the histological reconstruction of morphologies of some recorded neurons (**Supplementary Fig. 1b**), and is consistent with previous reports[22–24] that blind patch recording with large pipette opening sizes has a strong sampling bias toward excitatory neurons.

***In vivo* two-photon imaging-guided recording.** Two-photon imaging guided recordings were made from PV^+ neurons in viral injected *Pvalb-cre* tdTomato mice. *In vivo* two-photon imaging was performed with a custom-built imaging system as previously described[27,28]. A mode-locked Ti:sapphire laser (MaiTai Broadband, Spectra-Physics) was tuned at 880 nm with the output power at 50–300 mW for fluorescently labeled PV^+ cells in middle layers. For cell-attached recording, the glass pipette, with ~1-μm tip opening and 8–10-MΩ impedance, was filled with filtered ACSF containing 0.15 mM calcein (Invitrogen). The pipette tip was navigated in the cortex and patched onto a fluorescent soma as previously described[27,28]. After confirming a successful targeting, the positive pressure in the pipette (~10 mbar) was then released and a negative pressure (20–150 mbar) was applied to form a loose seal (with 0.1–0.5-GΩ resistance), which was maintained throughout the course of the recording. The depth of the patched cell was directly determined under imaging with *z* step control.

Auditory stimulation. To obtain the frequency tuning of excitatory synaptic currents, we delivered a pseudorandom sequence of pure tones (50-ms duration, 3-ms ramp, 2–32 kHz, 0.2 octave steps) without and with coupling of LED illumination (500-ms duration; starting from the onset of the sound stimulus) in an alternating pattern. The inter-stimulus interval was 5–10 s, corresponding to a 10–20-s interval between consecutive LED stimulation, which would allow a full recovery of ChR2 function from desensitization[29] (**Supplementary Fig. 1a**). LED illumination effectively evoked spikes of PV neurons in each of consecutive trials (**Supplementary Fig. 1a**), leading to effective silencing of spikes of excitatory neurons in each trial (**Fig. 1d**). Given the relatively long inter-stimulus interval, we tested frequency tuning mostly at one sound intensity (40~60 dB sound pressure level). For direction selectivity, logarithmic frequency-modulated stimuli sweeping between 0.5–64 kHz with a speed of 70 octave s^{-1} were generated and calibrated according to their output envelope[20]. Frequency-modulated sweeps

doi:10.1038/nn.3493

without and with coupling LED illumination were delivered in an alternating pattern. Sweep intensity was set at 50 dB sound pressure level.

Photostimulation. Blue (470 nm) fiber-coupled LED was used for photostimulation[30]. We tested optic fiber of different diameters, and mostly used 0.8-mm fiber (NA 0.39, Thorlabs) in our experiments. The fiber controlled by micromanipulator was positioned close to the surface of the exposed cortical region (~2 × 1.5 mm, covering the whole primary auditory region). The LED illuminated the entire exposed cortical surface. The LED was driven by a NIDAQ board (National Instruments) with a custom-made LabView software and was coupled with sound generation. For each experiment, loose-patch recordings from excitatory neurons were carried out to verify the effectiveness of cortical silencing. Both loose-patch and multi-unit recordings were carried out in the MGBv to test the effect of cortical silencing on the response properties of auditory thalamic neurons.

Tone-evoked response and onset latency. All the synaptic responses were averaged by trials. The peak synaptic responses were analyzed in a 10–50-ms time window after the tone onset; the integrated charge was calculated in a 0–200-ms time window. The onset latency of the average synaptic trace was identified at the time point in the rising phase of the response waveform, where the amplitude exceeded the average baseline level by 2 s.d. of the baseline fluctuation. Only responses with onset latencies within 7–40 ms of the onset of tone stimulus were considered as evoked.

Frequency tuning and direction selectivity. For frequency tuning of excitatory responses at a given tone intensity, the total effective frequency range (that is, tuning range) was determined by the frequency range for all the significantly evoked responses. Best frequency was defined as the frequency that evoked the maximum excitatory response. To quantify the half-maximum bandwidth of frequency tuning, an envelope curve (tuning curve) was generated using MATLAB software Envelope 1.1 (MathWorks) based on the peak amplitude or total charge of synaptic responses in the effective frequency range. The DSI was defined as $(R_1 - R_2)/(R_1 + R_2)$, where R_1 is the response magnitude at the preferred direction and R_2 is that at the null direction.

Statistics. Kolmogorov-Smirnov test (we used Lilliefors test, an adapted Kolmogorov-Smirnov test) and Shapiro-Wilk test (when sample size was smaller than 50) were first applied to exam whether samples had a normal distribution. In the case of a normal distribution (**Fig. 2e**), paired *t* test was applied. Otherwise (**Fig. 2c**), a non-parametric test (Wilcoxon signed-rank test) was applied. Statistics using the non-parametric and parametric tests led to the same conclusion in this study. Data were presented as mean ± s.d. if not otherwise specified. As the responses with and without cortical silencing were tested multiple (5–10) times, paired *t* test or Wilcoxon signed-rank test was also performed on an individual cell basis. The results were consistent with the group comparison.

21. Hackett, T.A., Barkat, T.R., O'Brien, B.M., Hensch, T.K. & Polley, D.B. *J. Neurosci.* **31**, 2983–2995 (2011).
22. Margrie, T.W., Brecht, M. & Sakmann, B. *Pflugers Arch.* **444**, 491–498 (2002).
23. Wehr, M. & Zador, A.M. *Nature* **426**, 442–446 (2003).
24. Zhou, M., Tao, H.W. & Zhang, L.I. *J. Neurosci.* **32**, 18068–18078 (2012).
25. Zhang, M. *et al. J. Neurosci.* **31**, 5460–5469 (2011).
26. Li, Y.T. *et al. J. Neurosci.* **32**, 16466–16477 (2012).
27. Liu, B.H. *et al. J. Neurosci.* **29**, 10520–10532 (2009).
28. Ma, W.P. *et al. J. Neurosci.* **30**, 14371–14379 (2010).
29. Lin, J.Y., Lin, M.Z., Steinbach, P. & Tsien, R.Y. *Biophys. J.* **96**, 1803–1814 (2009).
30. Adesnik, H., Bruns, W., Taniguchi, H., Huang, Z.J. & Scanziani, M. *Nature* **490**, 226–231 (2012).